

Geometric phase flat optical gratings with high diffraction angle based on dual frequency nematic liquid crystal

*Inge Nys**, *Sunqian Liu*, *Yu-Nung Huang*, *Olga Strzeżysz*, *Przemysław Kula* and *Kristiaan Neyts*

I. Nys, S. Liu, Y.-N. Huang, K. Neyts

Liquid Crystals and Photonics Group, Department of Electronics and Information Systems,
Ghent University,

Technologiepark-Zwijnaarde 126, 9052 Ghent, Belgium

E-mail: Inge.Nys@Ugent.be

O. Strzeżysz, P. Kula

Faculty of Advanced Technology and Chemistry, Military University of Technology, 00-908
Warsaw, Poland

Keywords: flat optical components, diffraction gratings, dual frequency liquid crystals, electrically tunable, optimized director configurations

Diffractive optical elements (DOEs) are increasingly used as lightweight and compact solutions in photonic devices. Steering of light and manipulation of the polarization can be efficiently obtained with the help of photo-aligned liquid crystal (LC) devices. We study one-dimensional LC diffraction gratings that are based on the geometric phase principle and demonstrate that the optical functionality can be substantially broadened by using dual frequency LC. Switching between a highly efficient diffractive and a transmissive state is obtained by adjusting the frequency of the applied electric field. Compared to commonly studied one-dimensional (1D) nematic LC diffraction gratings, the steering efficiency over large diffraction angles is strongly increased. By using an appropriate electric-field treatment, the efficiency for first order diffraction of red light over an angle of 12.6° increases from 60% to 90%. Moreover, additional switching phenomena are observed at intermediate voltage treatments, leading to enhanced tunability of the DOEs. The origin of this behavior is explained with the help of finite element Q-tensor simulations for the director configuration.

1. Introduction

Liquid crystal (LC) – based diffractive optical elements (DOEs) have attracted increasing attention over the last decades, especially since the discovery of LC DOEs that are based on the geometric phase principle. LCs, with their anisotropic optical properties and easily accessible electrical tunability, have been efficiently combined with photo-alignment patterning at the surfaces to demonstrate a multitude of flat optical components with diverse functionalities.^[1] Photo-alignment can impose a patterned optical axis orientation in the LC device that is translated into a geometric phase profile or so-called Pancharatnam-Berry (PB) phase profile.^[2] Gratings, lenses, beam splitters, etc. with high efficiency, compact design and lightweight have been demonstrated in this way and even made commercially available.^[3] This revolution has been enabled by the development of reliable photo-alignment techniques that allow to define close to arbitrary anchoring patterns at the surfaces with high resolution.^[4] A photosensitive alignment agent is deposited on top of an ITO coated substrate and the preferred optical axis orientation is defined by illumination with polarized light. The use of optical illuminations makes it possible to obtain high resolution without the need for complex manufacturing techniques such as electron-beam lithography. Typically UV or blue light is used to define the alignment pattern, enabling patterns with feature sizes of only a few hundred nanometer.^[5] Usually planar orientation with variable azimuthal anchoring angle is obtained, while the polar anchoring properties are not influenced by the illumination. Depending on the envisioned optical functionality, different illumination methods have been used, such as interference illumination (polarization holography),^[6] direct write illumination,^[7] and polarization projection imaging with the help of a digital micromirror device,^[8] plasmonic-mask,^[9] or spatial light modulator.^[10] For the one-dimensional (1D) diffraction gratings studied in this article, we used interference illumination with two circularly polarized light beams with opposite handedness.^[6a] A periodically rotating alignment pattern is introduced at the surface (the xy -plane), defined by $\mathbf{n}(x) = \sin\left(-\frac{\pi x}{\Lambda}\right) \mathbf{1}_x + \cos\left(-\frac{\pi x}{\Lambda}\right) \mathbf{1}_y$, with \mathbf{n} the optical axis (or director) orientation and Λ the alignment period over which the optical axis is rotating by 180° (**Figure 1**). Very efficient LC-based diffraction gratings have been demonstrated based on this approach, both in transmission or in reflection, depending on the type of LC that is used (non-chiral nematic liquid crystal (NLC) or chiral nematic liquid crystal (CLC) respectively). Research on NLC-based transmissive gratings was initiated in 2005 by Crawford et al.^[6a] while reflective gratings based on short pitch CLC have attracted attention in recent years.^[11]

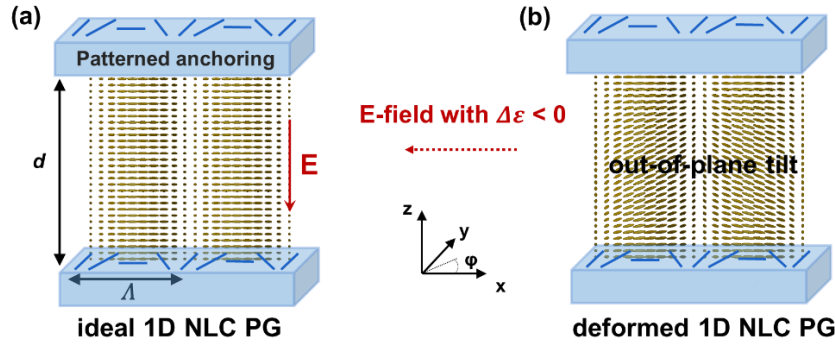


Figure 1. Schematic representation of an idealized director configuration (a) and a deformed director configuration in 1D NLC gratings with small Λ/d (b). Configuration (a) can be achieved from (b) by the application of a field, when the material has $\Delta\epsilon < 0$. Reproduced under terms of the CC-BY license.^[12b] 2021, Inge Nys, published by Taylor & Francis.

Diffraction over large angles with high efficiency has been demonstrated in reflective devices, but is difficult to achieve in devices that operate in transmission. Although the theoretical diffraction efficiency can reach 100% for circularly polarized light in the paraxial approximation (see section 5.1.), substantial deviations appear for larger diffraction angles. To a large extent this is caused by deviations of the director configuration from the ideal case. In the ideal configuration, the NLC director in the bulk simply follows the anchoring pattern at the substrates (Figure 1(a)), resulting in a patterned optical axis orientation that is uniform in the cell thickness. Uniformity of the director along the z -axis, however is only achieved in good approximation in thin cells, with a large alignment period Λ , with a large anchoring strength and for LC with limited elastic anisotropy (almost equal splay, twist and bend elastic constants). Faster variations in the director require higher elastic energy per unit volume and typically large deviations from the ideal alignment appear when the cell thickness d becomes comparable to or larger than the alignment period Λ .^[12] The half wave condition ($\Delta n \cdot d = \frac{\lambda}{2}$) specifies the minimal layer thickness for obtaining efficient diffraction, and therefore the requirement that the period Λ remains (substantially) larger than the cell thickness d , limits the maximum achievable diffraction angle. A lower diffraction efficiency inevitably occurs for structures with short period and large diffraction angle.

This critical thickness limitation has been identified in 2007 by Komanduri et. al.^[12a] and some efforts have been made to overcome this. Apart from the application of short pitch CLC to realize reflective gratings,^[11] the use of multi-layer spin-coating for transmissive devices has been proposed.^[13] In this case, multiple layers of polymerizable LC materials are spin-

coated and subsequently polymerized on top of each other. The individual layer thickness can in this way be limited, but the fabrication becomes far more complex, the electrical tunability is lost, the alignment at the air interface is not well-controlled and complex material mixtures are required. To improve the performance of transmissive LC gratings, also a dual-twist design was proposed, by adding a small amount of chiral dopant in the LC mixture. This allowed to obtain larger diffraction angles by depositing multiple layers of polymerizable chiral LC. ^[13a]

In this work we propose another solution to overcome the critical thickness limitation, that avoids multi-layer spin-coating and polymerizable LC mixtures. By using dual frequency nematic LC (with a negative dielectric anisotropy in a certain frequency range, above the cross-over frequency f_{co}), the simple device design can be maintained and the diffraction efficiency over large angles can be increased by applying a voltage over the LC layer. As far as we know, we are the first to demonstrate this concept. A fast-switching 1D grating with dual frequency LC has been reported before, but with a small diffraction angle ($< 1^\circ$), based on a large alignment period $\Lambda = 50 \mu\text{m}$ and a thickness well below the critical thickness. ^[14] In our solution, a simple cell geometry is used, with uniform indium tin oxide (ITO)-coated glass substrates at the top and bottom. Applying a voltage in the frequency range where the dielectric anisotropy is negative $f > f_{co}$, diminishes the out-of-plane tilt of the director and in this way restores the idealized planar rotating director configuration in the bulk of the cell (Figure 1), also for devices in which the critical thickness limitation is exceeded. Moreover, by using dual frequency LC, the frequency range with positive dielectric anisotropy ($f < f_{co}$) can be used to effectively tune the diffraction efficiency in different orders. Switching between highly efficient transmission ($> 85\%$ zeroth order diffraction) and highly efficient large angle diffraction ($> 90\%$ first order diffraction, over an angle of 12.6°) can be achieved with limited voltage application. Interestingly, for intermediate electric-field treatments in the negative dielectric anisotropy range ($f > f_{co}$), additional switching phenomena appear that allow to further extend the optical functionality of the device. In this manuscript, after describing the device design (section 2), the experimental demonstration of the device behavior (section 3) is followed by numerical simulations, to explain the origin of the observed phenomena (section 4). The results from simulations and experiments are compared in the discussion section (section 5).

2. Device design

The 1D LC diffraction gratings are produced in a standard cell geometry as described in more detail in the experimental section. The coated glass substrates are glued together ($d \approx 3 \mu\text{m}$) before the cell is exposed to photo-alignment illumination. A periodically rotating azimuthal anchoring pattern is imposed at the substrates, defined by $\varphi(x) = \frac{\pi}{2} - \frac{\pi x}{\Lambda}$ (Figure 1), with φ the azimuthal anchoring angle with respect to the x-axis (see Experimental section).

Anchoring patterns with different alignment periods ($\Lambda = 2.1 \mu\text{m}$, $2.9 \mu\text{m}$ and $3.9 \mu\text{m}$) are written at different areas in the same cell. The analysis is focused on the alignment period $\Lambda = 2.9 \mu\text{m}$, while the results for $\Lambda = 2.1 \mu\text{m}$ and $3.9 \mu\text{m}$ are mainly reported in the supporting information to provide a broader insight in the device behavior.

Table 1. Optical and dielectric properties of LC material mixture 1952H at 20°C.

Optical properties		Dielectric properties	
Clearing point	154.8°C	$\Delta\epsilon$ (at 1 kHz)	1.37
Δn (at 589 nm)	0.1	ϵ_{\parallel}	6.45
n_o	1.48	ϵ_{\perp}	5.08
n_e	1.58	$\Delta\epsilon$ (at 1 MHz)	-2.10
		ϵ_{\parallel}	3.00
		ϵ_{\perp}	5.10
		f_{co}	1.74 kHz

After photo-alignment processing, the cell is filled above the clearing temperature with the dual frequency NLC mixture 1952H (prepared at Warsaw Military University, Poland) being the modification of mixtures AB1 previously reported by Dabrowski et al.^[15] After the filling is completed, the cell is cooled down to room temperature and observed by polarizing optical microscopy (Nikon Eclipse E400 POL) and diffraction measurements. The material specifications (dielectric properties and optical properties) for mixture 1952H at 20°C are summarized in **Table 1** while the temperature and frequency dependence of the dielectric constants are shown in **Figure 2**. The cross-over frequency f_{co} at 20°C is $f_{co} = 1.74 \text{ kHz}$, with a positive dielectric anisotropy appearing at lower frequencies $f < f_{co}$ ($\Delta\epsilon = 1.37$ at 1 kHz) and a negative dielectric anisotropy appearing at higher frequencies $f > f_{co}$ ($\Delta\epsilon = -2.1$ at 1 MHz). Experimentally, electric-fields with two different frequencies (1 kHz and 4 kHz) are applied to test the electric-field induced switching in both regimes. Dielectric properties of

dual frequency nematics and molecular dynamics in general are sensitive to temperature, with the cross-over frequency f_{co} shifting to higher values for increasing temperatures. The temperature in the lab was fluctuating within the interval [21°C, 23°C] during the measurement period and no additional temperature control for the LC cell was used. Although the dielectric anisotropy was not accurately measured, the 1 kHz and 4 kHz frequencies were always in the positive, respectively negative dielectric anisotropy range.

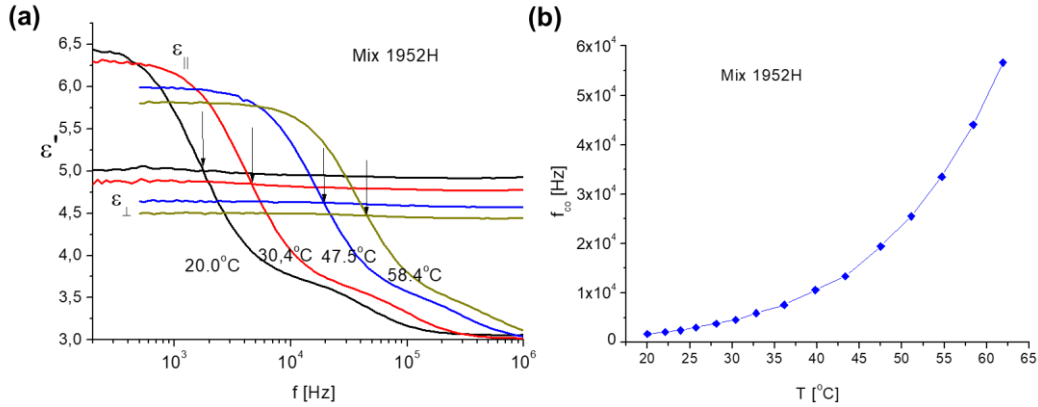


Figure 2. (a) Dielectric properties of the LC mixture 1952H as a function of the frequency for four different temperatures between 20°C and 58.4°C . (b) Cross-over frequency f_{co} for LC mixture 1952H as a function of the temperature.

3. Experimental observations

3.1. Polarizing optical microscopy images

After cooling down to room temperature, the cell was observed by polarizing optical microscopy (POM) between two crossed (or parallel) polarizers. Different voltages are applied to the cell, both at a frequency of 1 kHz ($\Delta\epsilon > 0$) and 4 kHz ($\Delta\epsilon < 0$). The results for the grating with $\Lambda = 2.9 \mu\text{m}$ are summarized in **Figure 3** while additional images are given in the supporting information (**Figure S1**) and the discussion section. Without applied voltage, a periodic line pattern is observed, with alternating bright and dark lines between crossed polarizers. In the idealized picture (Figure 1(a)), regions with a surface anchoring orientation $\varphi(x) \approx n\frac{\pi}{2}$ (with n and integer number) along the analyzer or the polarizer (x - or y -axis respectively), give rise to a dark line in transmission between crossed polarizers while regions with $\varphi(x) \approx \frac{\pi}{4} + n\frac{\pi}{2}$ give rise to a bright line. Neighboring bright lines are shifted over a distance $\Lambda/2$. The brightness and color of the bright lines are defined by the optical retardation and in the ideal director configuration (Figure 1(a)) they should be equal, resulting in a $\Lambda/2$ period in the optical transmission image at 0V. It is however clear that this condition is not

satisfied at 0V in our experiments and that deviations from the ideal configuration appear (Figure 3(a)). This will be further investigated in the discussion section (5.4).

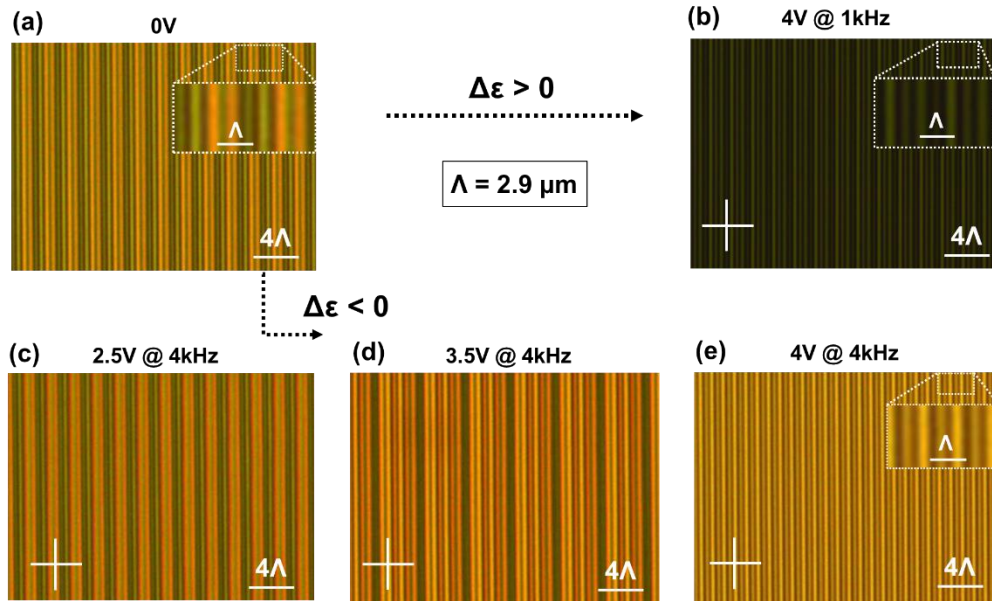


Figure 3. POM images between crossed polarizers for different applied voltages in the positive (b) and negative dielectric anisotropy range (c-e) for the 1D grating with alignment period $\Lambda = 2.9 \mu\text{m}$.

Applying a voltage at 1 kHz frequency ($\Delta\epsilon > 0$) between the top and bottom electrode gives rise to reorientation of the LC director towards the surface normal (z-axis). This results in a decreased retardation ($\Gamma = d \cdot \Delta n(V)$) and a lower transmission when the cell is observed between crossed polarizers (Figure 3(b)). Similar observations are made for the different alignment periods Λ , as shown in the supporting information (Figure S1).

Applying a voltage at 4 kHz frequency ($\Delta\epsilon < 0$) on the other hand results in a reorientation of the LC bulk director towards a planar director orientation (perpendicular to the electric-field lines). The POM images in Figure 3(d-e) and Figure S1 at 4 kHz show different results for different alignment periods. For the largest alignment period $\Lambda = 3.9 \mu\text{m}$, the images hardly change upon increasing the voltage and the observed periodicity remains equal to Λ , with a color difference observed between different bright lines (Figure S1(a)). For the area with intermediate alignment period $\Lambda = 2.9 \mu\text{m}$ (Figure 3), several transitions are observed for increasing voltages and the resulting period of the optical pattern is varying (from 2Λ to 4Λ and subsequently to $\Lambda/2$ between crossed polarizers). When taking a closer look at the images (Figure 3(a)), it is observed that darker regions (with $\sim\Lambda$ width) in the POM images gradually

disappear for increasing voltages. At high voltages ($4 V_{\text{rms}}$), the POM image closely represents the expected image between crossed polarizers for the ideal director configuration: alternating bright and dark lines with distance $\Lambda/2$ between subsequent bright lines (Figure 3(e)). For the smallest alignment period $\Lambda = 2.1 \mu\text{m}$ (Figure S1 (b)), the transmitted intensity changes slightly for increasing voltages (at 4 kHz), but no change in POM image period is observed (always 2Λ). In contrast to what is observed for the cell with alignment period $\Lambda = 2.9 \mu\text{m}$ (Figure 3), the overall brightness of the POM image for the $\Lambda = 2.1 \mu\text{m}$ structure is continuously decreasing for increasing voltage ($\Delta\varepsilon < 0$, Figure S1(b)), indicating that the director configuration is not evolving towards the ideal director configuration.

3.2. Diffraction measurements

Figure 4 shows experimental diffraction results (see methods section 7.) for alignment period $\Lambda = 2.9 \mu\text{m}$, while results for the other alignment periods are given in the supporting information (**Figure S2**). It is clear that the diffraction pattern can be strongly tuned by applying an electric-field with a 1 kHz frequency ($\Delta\varepsilon > 0$) or a 4 kHz frequency ($\Delta\varepsilon < 0$). In the absence of a voltage, the area with alignment period $\Lambda = 2.9 \mu\text{m}$ diffracts approximately 60% of the light into the -1^{st} order while the 0 order diffraction efficiency is approximately 20% (Figure 4). The power in the 0^{th} order is respectively smaller/larger for patterned areas with a longer/shorter alignment period ($\Lambda = 3.9 \mu\text{m}$ and $\Lambda = 2.1 \mu\text{m}$, Figure S2). Without applied voltage, there is even some diffraction in the $+1^{\text{st}}$ order (instead of the -1^{st} order) for $\Lambda = 2.1 \mu\text{m}$ (Figure S2). By applying a voltage of 1 kHz ($\Delta\varepsilon > 0$), the power in the -1^{st} order diffraction is decreasing while the 0^{th} order transmission power is increasing, due the reduction in retardation (starting from a retardation below a halve wave at 0V).

Interesting observations are made when an electric field with 4 kHz frequency is applied ($\Delta\varepsilon < 0$), because for $\Lambda = 3.9 \mu\text{m}$ and especially $\Lambda = 2.9 \mu\text{m}$ a sufficiently high voltage ($\geq 4V_{\text{rms}}$) leads to a clear increase in the -1^{st} diffraction order (Figure 4 and Figure S2). Some modulation in the diffraction efficiencies are observed as well for $\Lambda = 2.1 \mu\text{m}$ (Figure S2), but in this case the -1^{st} order diffraction efficiency is not increased at higher voltages. For the largest alignment period $\Lambda = 3.9 \mu\text{m}$ the increase in diffraction efficiency, when applying a voltage (for $\Delta\varepsilon < 0$), is limited to less than 10%, but for $\Lambda = 2.9 \mu\text{m}$ the -1^{st} order efficiency is increased from 60% to 90% (for a voltage $> 4 V_{\text{rms}}$). At intermediate voltages a strong modulation in the diffraction pattern is observed for the area with $\Lambda = 2.9 \mu\text{m}$, with additional diffraction orders appearing (Figure 4). The voltage at which this occurs is sensitive to the temperature. At 0V, the diffraction is mainly in the 0^{th} , -0.5^{th} and -1^{st} orders,

while at high voltages the diffraction is predominantly in the -1^{st} diffraction order. At intermediate voltages (around $3 V_{\text{rms}}$), the occurrence of the period 4λ (observed in the POM images in Figure 3) leads to a series of additional diffraction orders, such as the -0.25^{th} and -0.75^{th} orders (Figure 4(b)). Multiple experiments confirm that these results are reversible and not strongly dependent on the time of modulation (several seconds up to minutes).

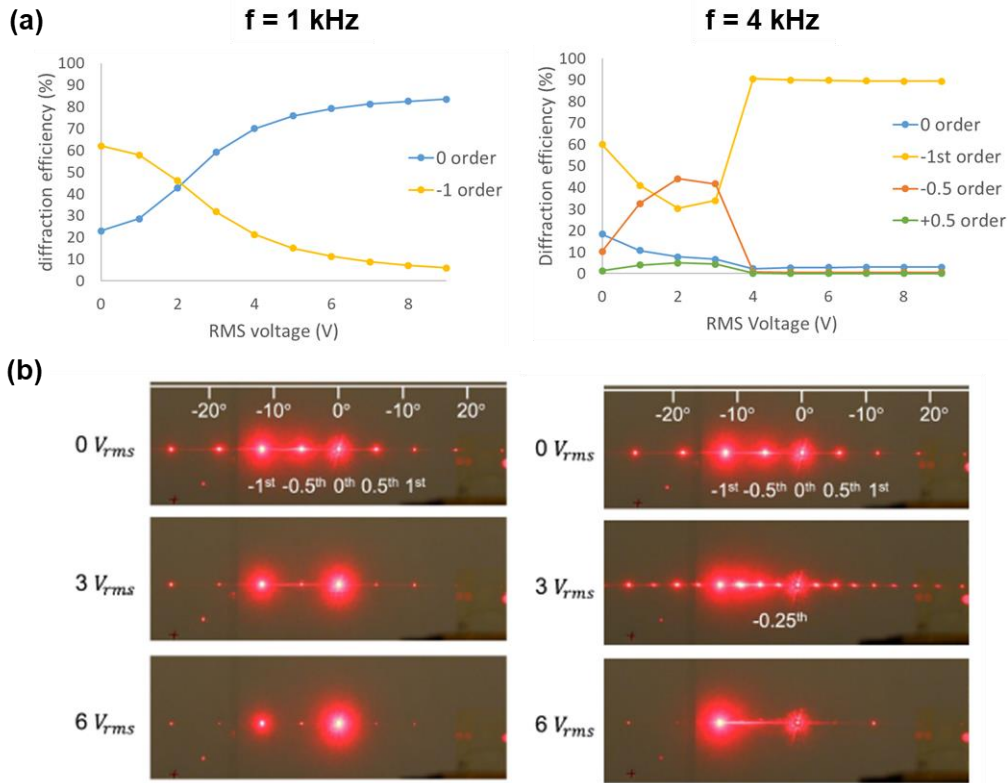


Figure 4. (a) Experimentally measured diffraction efficiencies as a function of the voltage in different diffraction orders, for frequencies 1 kHz ($\Delta\varepsilon > 0$) and 4 kHz ($\Delta\varepsilon < 0$) of the applied electric field. Measurements for alignment period $\lambda = 2.9 \mu\text{m}$ are shown. (b) Diffraction patterns captured on a black screen behind the LC cell for $\lambda = 2.9 \mu\text{m}$, for two frequencies (1 kHz and 4 kHz) of the applied electric field and three voltages ($0 V_{\text{rms}}$, $3 V_{\text{rms}}$ and $6 V_{\text{rms}}$).

4. Numerical simulations

Numerical simulations can be very helpful to elucidate the director configuration that produces the observed POM images and diffraction patterns. For this purpose, finite element Q-tensor simulations for the director configuration have been performed in combination with optical simulations (see methods section 7).

4.1. Finite element Q-tensor simulations for the director configuration

The simulated configurations (for $\Lambda = 2, 3$ or $4 \mu\text{m}$) without applied voltage show a 2Λ period for the director configuration (**Figure 5-7**). The director does not remain planar in the volume and an out-of-plane tilt is introduced. The tilt angle θ (w.r.t. the xy -plane) in the mid-plane is fluctuating around 58° for $\Lambda = 4 \mu\text{m}$, 64° for $\Lambda = 3 \mu\text{m}$ and 69° for $\Lambda = 2 \mu\text{m}$ with the smallest tilt observed in the regions with the surface director along the y -axis. The total elastic energy in the bulk of the layer is strongly reduced by introducing an out-of-plane tilt, as can be seen in **Figure S3** (by comparing the idealized and simulated configuration in respectively (a) and (b)). When directors in this configuration are represented by points on a unit sphere (**Figure 6(e)**), a large part of the sphere is filled up, leaving only an opening around the z -axis (director perpendicular to the substrate). The strong deviation from the planar bulk director configuration indicates that the grating thickness is well beyond the critical value.^[12a]

The simulated configurations (**Figure 5-7(b)**) with applied voltage in the positive dielectric anisotropy range ($\Delta\epsilon = 1.37$) confirm the well-known behavior with increasing out-of-plane tilt in the bulk for higher voltages. The unit sphere S^2 is practically completely filled, with many directors more or less parallel to the z -axis (**Figure 6(f)**).

Voltage application in the negative dielectric anisotropy range ($\Delta\epsilon = -1$) shows the envisioned effect of a near-to-ideal planar director configuration at high voltages (10 V, **Figure 5-7 (d)** and **Figure 6(h)**) for the three simulated alignment periods ($\Lambda = 2, 3$ or $4 \mu\text{m}$), but not at intermediate voltages (**Figure 5-7(c)**). At intermediate voltages (**Figure 5-7 (c)**) an interesting behavior is observed: instead of monotonically decreasing the tilt angle in the entire volume of the device for increasing voltages, localized regions with vertical director orientation are observed. In this case (**Figure 7(f,g)**) there is still a hole in the director distribution over the unit sphere, but it is displaced from its original location around the z -axis. While the director tilt in most regions is decreasing, there are regions with width $\sim\Lambda$ in which the tilt increases. These regions with high tilt are present closer to the top and closer to the bottom substrate. For $\Lambda = 2 \mu\text{m}$ two such regions are introduced at 5V in the 4Λ simulation area (**Figure 7(c)**), while for larger simulated alignment periods ($\Lambda = 3$ or $4 \mu\text{m}$) only one such region appears at 5 V (**Figure 5-6 (c)**).

The driving force for this transition at intermediate voltages in the negative dielectric anisotropy range can be understood by looking at **Figure 7(f)**. The mid-plane director configuration has a small tilt angle that lowers the dielectric energy, while the mid-plane azimuthal angle is fluctuating in a limited range (between -35° and $+10^\circ$ in **Figure 7(f)**), instead of following the continuous 4π rotation of the director at the surfaces. This is also illustrated by the representation of directors on the unit sphere in **Figure 7(f)**, in which the

mid-plane directors (in red) are confined to a small area close to the xy -plane. This behavior lowers both the elastic energy and the dielectric energy density near the mid-plane region. However, there is an increase in energy density around the localized regions with a close-to-vertical director near the top and the bottom substrates (Figure S3(c)). Remark that, if the simulation for 10V ($\Delta\varepsilon = -1$) is initiated from the director configuration at 5V (Figure 7(c,f)), another metastable (local minimum in the free energy) solution can be found (Figure 7(e,g)). This solution deviates strongly from the result in Figure 7(d), but, as will be discussed in section 5, experimental results indicate that the configuration in Figure 7(e,g) can indeed show up.

All in all, it is clear that the director configuration that is formed will depend on a delicate interplay between elastic, dielectric and surface anchoring effects. Our simulations do not aim to provide quantitative results for the director configurations at all voltages (as the materials parameters for the LC mixture 1952H, surface anchoring strength, etc. are not well known), but provide qualitative insight in the LC device behavior.

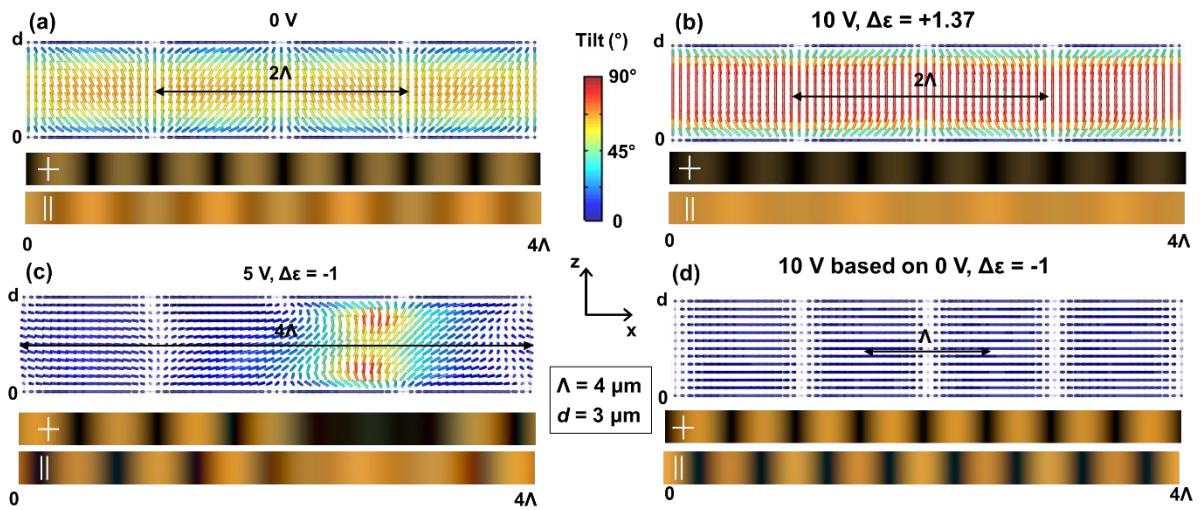


Figure 5. Simulation results for the director configuration and POM images (between crossed and parallel polarizers) for grating period $\Lambda = 4 \mu\text{m}$ and cell thickness $d = 3 \mu\text{m}$. The results are shown at 0 V (a), at 10 V for $\Delta\varepsilon = 1.37$ (b), at 5 V for $\Delta\varepsilon = -1$ (c) and at 10 V for $\Delta\varepsilon = -1$ (d). The color in the director configuration represents the tilt angle, with red/blue indicating respectively a vertical/horizontal director orientation.

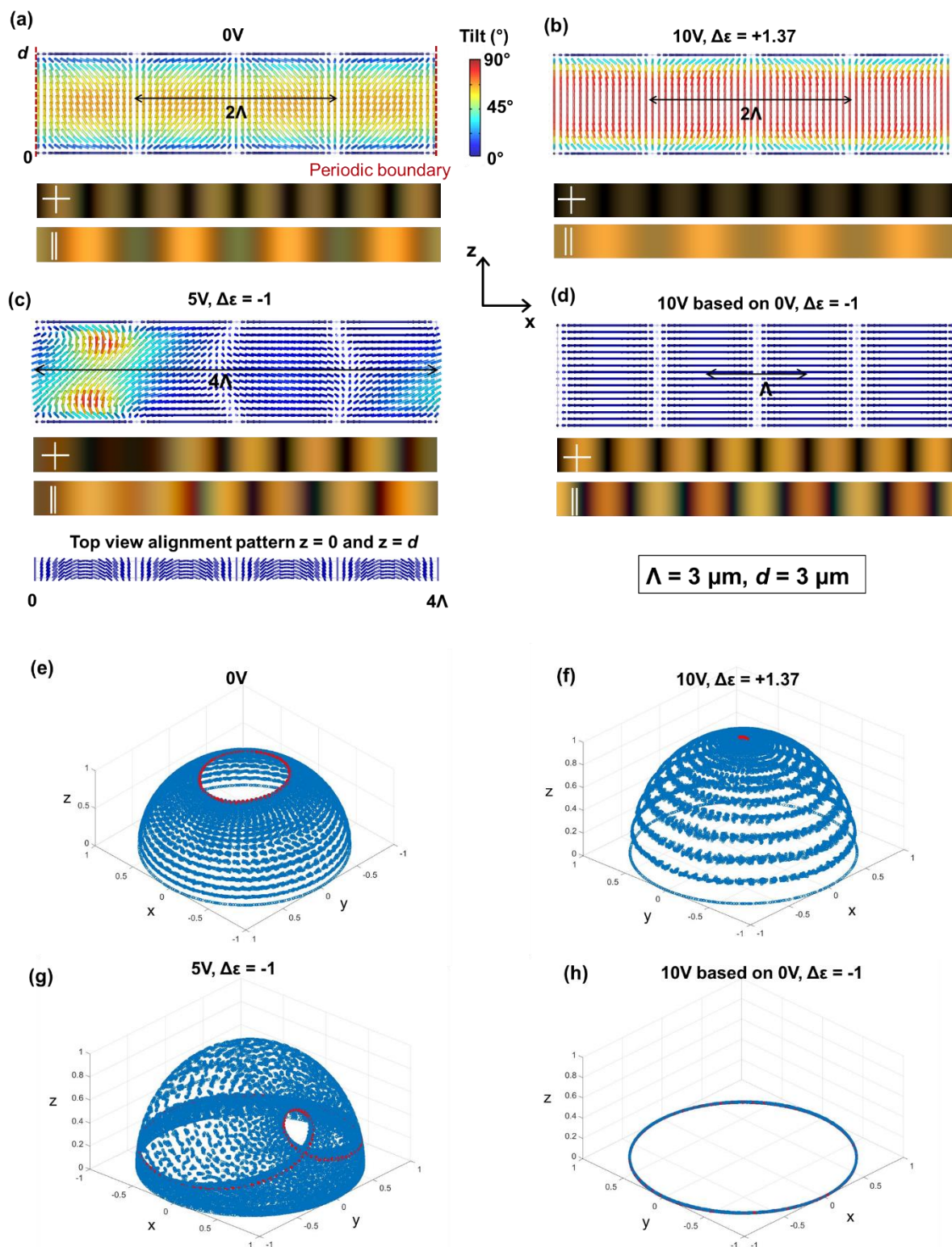


Figure 6. Simulation results for the director configuration and POM images (between crossed and parallel polarizers) for grating period $\Lambda = 3 \mu\text{m}$ and cell thickness $d = 3 \mu\text{m}$ (a-d). The corresponding representations of the director on the unit sphere are shown in (e-h), with points in the mid-plane represented in red and other points represented in blue. The results are shown at 0 V (a,e), at 10 V for $\Delta\epsilon = 1.37$ (b,f), at 5 V for $\Delta\epsilon = -1$ (c,g) and at 10 V for $\Delta\epsilon = -1$

(d,h). The color in the director configuration (a-d) represents the tilt angle, with red/blue indicating respectively a vertical/horizontal director orientation.

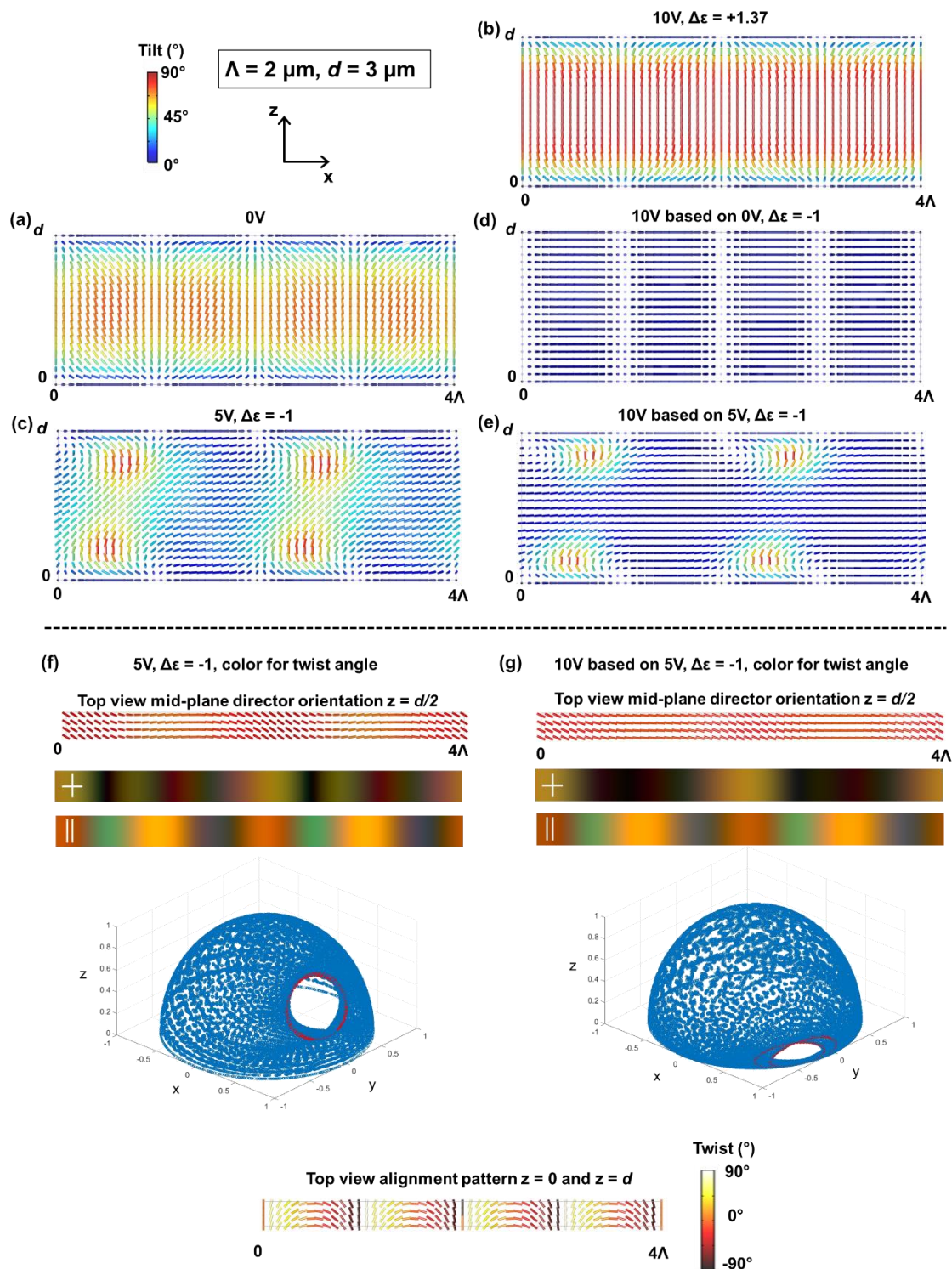


Figure 7. Simulation results for the director configuration at different voltages for a grating period $\Lambda = 2 \mu\text{m}$ and cell thickness $d = 3 \mu\text{m}$. For the configurations in (c) and (e), the mid-plane director is shown in (f) and (g) together with the simulated POM images and a representation of the director on the unit sphere, with points in the mid-plane represented in

red and other points represented in blue. In the director configurations, the color represents the tilt angle with respect to the xy -plane in (a-e) and the twist angle w.r.t. the x -axis in (f-g). The results are shown for 0 V (a), for 10 V with $\Delta\varepsilon = 1.37$ (b), for 5 V with $\Delta\varepsilon = -1$ (c, f) and for 10 V with $\Delta\varepsilon = -1$ (d,e,g). The results in (e) and (g) correspond to an alternative (metastable) solution that is found in the simulations after increasing the voltage to 10 V with $\Delta\varepsilon = -1$ starting from an initial condition that corresponds to the end result at 5 V (c,f).

4.2. Diffraction patterns and simulated transmission images

Based on the simulated director configuration, the near-field transmission between crossed (or parallel) polarizers is calculated with the help of open source software Nemaktis (<https://github.com/warthan07/Nemaktis>). Optical micrographs are simulated with the help of a generalized beam propagation method for propagation of the optical fields in birefringent media, as introduced by Poy et al. ^[16] The measured refractive indices at $\lambda = 589$ nm (Table 1) for the LC mixture 1952H are taken into account in the optical simulations and the results are included in Figures 5-7. Remark that the period observed in the director configuration often does not correspond with the period in the simulated POM images between crossed polarizers. This is because a 90° azimuthal rotation of the director gives rise to the same optical transmission between crossed polarizers, when the amplitude of the out-of-plane tilt is not changed.

The simulated 0V configuration (for $\Lambda = 2, 3$ or $4 \mu\text{m}$) shows a 2Λ period for the director configuration but a smaller period in POM, with subsequent bright (or dark) lines separated by a distance $\Lambda/2$. The simulated high voltage state for $\Delta\varepsilon < 0$ (Figure 5(d), Figure 6(d)) shows another transmission color but otherwise similar image in POM, although the spatial period for the director configuration is Λ in this case (w.r.t. 2Λ at 0V). At intermediate voltages for $\Delta\varepsilon < 0$, the simulated director configuration and the resulting POM images show a 4Λ spatial period for $\Lambda = 3$ or $4 \mu\text{m}$ (Figure 5(c), Figure 6(c)) and a 2Λ spatial period for $\Lambda = 2 \mu\text{m}$ (Figure 7(f)).

The far-field diffraction pattern is found with the help of a Fast Fourier Transform (FFT) of the near-field transmission. This calculation is limited to one wavelength ($\lambda = 633$ nm) and the near-field calculation of the phase and polarization state after propagating through the LC, is again performed with the help of the open source software Nemaktis. ^[16] The wave is decomposed into two waves with orthogonal linear polarizations (along the x - and y -axis) and a 1D FFT is performed for both near-field components. The polarization state and the

diffraction intensity in the different orders is found by combining the two diffraction patterns. The simulated diffraction patterns for right handed circularly polarized incident light and different applied voltages are shown in **Figure 8**.

The simulated director configuration at 0V gives rise to substantial diffraction in the 0th and -1st order, with no other diffraction orders observed. The portion of light that is transmitted into the zeroth order is larger for a smaller alignment period Λ (Figure 8). The simulated medium voltage state (5V) for $\Delta\epsilon = -1$ shows some intensity in the 0th, -0.25th, -0.75th, -1st and +0.25th diffraction orders for $\Lambda = 3$ and 4 μm , and redirection of light into the half-integer orders (0th, -0.5th, -1st and +0.5th) for $\Lambda = 2$ μm . At high voltages (10 V), simulations with negative dielectric anisotropy show efficient redirection of light in the -1st diffraction order, with all other orders being negligible (for $\Lambda=2$ μm , only the configuration of Fig.7(d) is represented). High voltages for positive dielectric anisotropy on the other hand give rise to predominant transmission into the 0th order.

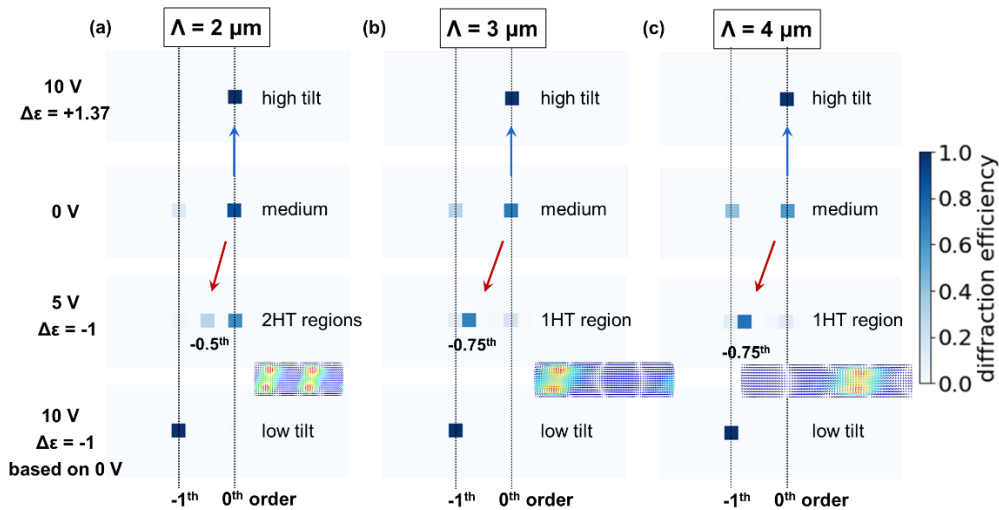


Figure 8. Simulation results for the diffraction efficiency at different voltages for gratings with a period Λ of 2 μm (a), 3 μm (b), 4 μm (c) and right handed circularly polarized incident light. From top to bottom: 10 V for $\Delta\epsilon = +1.37$ (blue arrow); 0 V; 5 V for $\Delta\epsilon = -1$; 10 V for $\Delta\epsilon = -1$ (red arrow). For each state the tilt is described: low, medium, high, 1 or 2 high tilt (HT) regions in a 4Λ unit cell. For 5 V ($\Delta\epsilon = -1$) a drawing of the director configuration is included.

5. Discussion

5.1. theoretical background

To describe the diffraction behavior of idealized 1D NLC diffraction gratings (Figure 1(a)), the theoretical framework developed by Escuti et al. can be used.^[17] The optical diffraction of a 1D gratings with spatially varying in-plane uniaxial birefringence can be described in the paraxial approximation by the following equations: $\mathbf{D}_m = \frac{1}{\Lambda} \int_0^\Lambda \mathbf{T}(\mathbf{x}) \mathbf{E}_{in} \exp(-i2\pi m x / \Lambda) dx$, with \mathbf{D}_m the far-field electric field for diffraction order m , Λ the alignment period (defining a π rotation of the azimuthal orientation) and $\mathbf{T}(\mathbf{x}) \mathbf{E}_{in}$ the near-field transmission of the diffraction grating. $\mathbf{T}(\mathbf{x})$ described the spatially variable Jones matrix, taking into account the local birefringence associated with the 1D grating. When an ideal bulk LC director configuration is assumed (as in Figure 1(a)), following the surface anchoring orientation in the bulk, it follows that $\mathbf{D}_m = 0$ for $m \geq 2$, and that the diffraction efficiencies $\eta_m = |\mathbf{D}_m|^2 / |\mathbf{E}_{in}|^2$ in the zeroth and +/- first order are $\eta_0 = \cos^2\left(\frac{\pi \Delta n d}{\lambda}\right)$ and $\eta_{\pm 1} = \frac{1}{2} [1 \pm S'_3] \sin^2\left(\frac{\pi \Delta n d}{\lambda}\right)$, with λ the wavelength of the incident light, S'_3 the normalized Stokes parameter corresponding to the ellipticity of the light and Δn the birefringence of the LC. For circularly polarized light, this means that theoretically 100% of the light is redirected into the first diffraction order if the half wave condition $\Delta n d = \frac{\lambda}{2}$ is met. The LC layer thickness in our cell ($d = 3.2 \mu\text{m}$) was chosen to meet the half wave condition for red light. This explains why the first order diffraction efficiency is monotonously decreasing for increasing voltages in the positive dielectric anisotropy range (1 kHz, Figure 4 and Figure S2). The birefringence $\Delta n d$ decreases below $\frac{\lambda}{2}$ for increasing voltages and the first order efficiency decreases while the zeroth order efficiency increases. These observation are in agreement with earlier reports related to 1D NLC gratings with positive dielectric anisotropy and will not be further discussed.^[17]

The theoretical results described above are valid in the paraxial approximation, for the idealized director configuration and for thin gratings ($\frac{2\pi \lambda d}{n_0 \Lambda^2} < 1$). Excellent agreement with this theory has been demonstrated before for gratings with large alignment period Λ , but strong deviations have been shown to occur for gratings with a small alignment period Λ . Although a small alignment period Λ sets limitations on the use of the paraxial approximation and the thin grating theory^[18], an important deviation also occurs due to changes in the bulk director configuration.^[12a] This is indirectly demonstrated by our experiments, that show a strong increase of the first order diffraction efficiency upon application of a voltage with frequency in the negative dielectric anisotropy range (see section 5.2).

5.2. High voltage application in the negative dielectric anisotropy range (4 kHz)

The smaller Λ (w.r.t. d), the larger the deviation from the ideal bulk director configuration at 0V and the lower the first order diffraction efficiency (Figure 4, Figure S2, Figure 8).

However, for sufficiently high applied voltages at 4 kHz, a high first order diffraction efficiency is experimentally observed for the gratings with $\Lambda = 2.9 \mu\text{m}$ and $\Lambda = 3.9 \mu\text{m}$ (Figure 4, Figure S2). This indicates that the electric-field helps to restore the ideal director configuration and to approximate the requirements for high diffraction efficiency (section 5.1.). In general, applying a voltage at 4 kHz ($\Delta\varepsilon < 0$) is expected to result in a reorientation of the LC bulk director towards a planar director orientation, perpendicular to the electric field.

For the largest alignment period $\Lambda = 3.9 \mu\text{m}$ the increase in efficiency is limited to less than 10% since the out-of-plane tilt in the 0V configuration is not yet very pronounced. For $\Lambda = 2.9 \mu\text{m}$ on the other hand the -1st order efficiency increases from 60% to 90% by applying a $\geq 4 \text{ V}_{\text{rms}}$ voltage (4 kHz). Both POM and diffraction results make clear that for the area with $\Lambda = 2.9 \mu\text{m}$, the ideal director configuration of Figure 1(a) is obtained for high voltages with frequency in the negative anisotropy range. In this case a sequence of bright (and dark) lines with $\Lambda/2$ separation is observed by POM and there is a strong first order diffraction efficiency. The experimental observations (POM and diffraction) for $\Lambda = 2.9 \mu\text{m}$ and $\Lambda = 3.9 \mu\text{m}$ at a high voltage with $\Delta\varepsilon < 0$ are therefore well understood by numerical simulations (Figure 5(d), Figure 6(d), Figure 8) and by the approximate theoretical description (section 5.1.).

For the grating with $\Lambda = 2.1 \mu\text{m}$ the behavior upon application of a 4kHz ac voltage is quite different. Some modulation in the diffraction efficiency is observed (Figure S2), but the first order diffraction efficiency is not increased at higher voltages and the overall brightness of the POM image is decreased (Figure S1). Based on these observations, it is clear that the structure is no longer evolving towards the ideal director configuration for increasing voltages (for $\Delta\varepsilon < 0$). The electric-field treatment does not differentiate between different azimuthal director orientations but only reduces the tilt angle in the bulk. When the anchoring strength is not strong enough or the contribution of the bulk elastic energy becomes too large to maintain a periodically rotating director orientation in the bulk, electric-field treatment can no longer induce the ideal bulk director configuration. The reason for this is that, for small values of Λ , the splay $\frac{1}{2} K_{11} \frac{\pi^2}{\Lambda^2} \cos^2\left(\frac{\pi}{\Lambda} x\right)$ and bend $\frac{1}{2} K_{33} \frac{\pi^2}{\Lambda^2} \sin^2\left(\frac{\pi}{\Lambda} x\right)$ elastic energy densities become very high and the formation of the ideal grating structure is not possible, even when a voltage

is applied in the $\Delta\varepsilon < 0$ range. Applying a 4 kHz voltage to the cell in this case results in the structure presented in Figure 7(e,g) or in the creation of twist disclination lines close to the surfaces, combined with a more or less uniformly oriented planar director configuration in the middle of the LC layer. A decrease in brightness in POM images at high voltages (4 kHz) can be linked to a more predominant orientation of the bulk LC director along the analyzer or the polarizer, as shown in Figure 7(g). This simulation result is obtained when starting with the initial condition of the director configuration for 5V (Figure 7(c)), which is a different from the simulation result of Figure 7(d) obtained when starting the simulation from the 0V solution (Figure 7(a)). It is clear that experimentally we observe only the configuration of Figure 7(e,g) at high voltages for $\Lambda = 2.1 \mu\text{m}$, with the mid-plane director roughly along the x-axis, independently from the voltage treatment.

This makes clear that the proposed solution, to obtain highly efficient large angle diffraction by applying a voltages in the negative dielectric anisotropy range, is only valid for a certain range of grating periods. When Λ is too small and the critical thickness is exceeded by too large of an amount, the electric field treatment is no longer able to introduce the ideal bulk configuration. However, is clear that the minimum value for Λ/d to obtain high diffraction efficiency can be substantially reduced by applying a voltage over an LC mixture with negative dielectric anisotropy. The corresponding maximal diffraction angle with high efficiency will depend on the LC material properties (dielectric properties, birefringence and elastic constants) and the anchoring strength provided by the surface alignment layers (in this work we use brilliant yellow, which may have a lower anchoring strength than SD1^[14]).

5.3. Medium or low voltage application in the negative dielectric anisotropy range (4 kHz)

For the largest alignment period $\Lambda = 3.9 \mu\text{m}$ a smooth transition between the low voltage and high voltage state ($\Delta\varepsilon < 0$) is observed both in POM and diffraction measurements (Figure 3 and 4) . This confirms that a continuous decrease of the LC bulk tilt angle for increasing voltages in the negative dielectric anisotropy range is at the basis of the observed behavior. This is different for the gratings with smaller alignment period $\Lambda = 2.1 \mu\text{m}$ or $2.9 \mu\text{m}$. We focus on the results for the alignment period $\Lambda = 2.9 \mu\text{m}$, where the ideal configuration with high first order diffraction efficiency is obtained at high voltages, but only after an abrupt transition at intermediate voltages. The simulations (section 4) suggest that at intermediate voltages an additional phenomenon can appear, giving rise to alternating regions with low and high average director tilt in the bulk of the layer (see figure 5-7(c)). In POM

images between crossed polarizers, regions with a large average tilt angle give rise to a lower transmission (dark) while the other regions consist of alternating bright and dark stripes as in the standard configuration. The simulations for $\Lambda = 3 \mu\text{m}$ at 5V show a 4Λ period in which the director configuration above one alignment period Λ has transformed into a strongly tilted configuration (Figure 6(c)). In this region, the π azimuthal rotation at the substrates is lifted in the middle of the layer, by introducing regions with alignment near the z-axis close to the top and bottom substrate. Simulations for $\Lambda = 2 \mu\text{m}$ (Figure 7(c,e,f,g)) show that a configuration in which two (out of four) regions with width $\sim\Lambda$ are transformed in this way, is also possible. The spatial period becomes 2Λ instead of 4Λ in this case. Remark that symmetry breaking occurs in this medium voltage range for $\Lambda = 2.1 \mu\text{m}$ or $2.9 \mu\text{m}$: different equivalent positions in the (2Λ or respectively 4Λ) unit cell can be chosen and the resulting azimuthal distribution in the mid-plane is asymmetric (e.g. fluctuating between 10° and -35° in Figure 7(f)). The actual director configuration that is formed depends on a delicate balance involving the applied electric field, the dielectric and the elastic constants of the material and the parameters for the surface anchoring treatment. It is clear that regions with a strong out-of-plane tilt can be recognized by POM between crossed polarizers (rather dark transmission) or by diffraction experiments. The presence of a 2Λ or 4Λ period in the director configuration gives rise to additional diffraction orders, such as half orders $\pm 0.5, 1.5, \dots$ or quarter orders $\pm 0.25, 0.75, 1.25$.

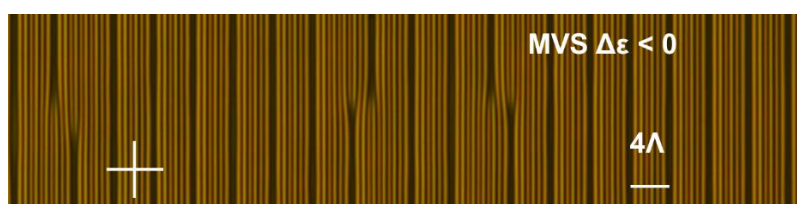


Figure 9. POM image between crossed polarizers, oriented along the x- and y-axis, for the alignment period $\Lambda = 2.9 \mu\text{m}$ in the medium voltage state for an applied voltage with 4 kHz frequency ($\Delta\epsilon < 0$). A region is selected in which some shifted domains can be observed.

At medium voltages a 4Λ spatial period is experimentally observed by POM for $\Lambda = 2.9 \mu\text{m}$, with one $\sim\Lambda$ wide dark region present per 4Λ spatial period (Figure 3(a)). This is combined with a diffraction pattern that contains $\pm 0.25^{\text{th}}, 0.75^{\text{th}}, 1.25^{\text{th}}$ diffraction orders in addition to the $0^{\text{th}}, -0.5^{\text{th}}, -1^{\text{st}}$ diffraction orders appearing at 0V (Figure 4). Both observations correspond to the simulations at intermediate voltages for $\Lambda = 3 \mu\text{m}$ (Figure 5, 8). The experimental distribution of light into the different diffraction orders deviates from the simulated results

(Figure 8(b)), which can be linked to symmetry breaking and the formation of domains in which the dark lines are shifted, as illustrated in the POM image in **Figure 9**. This is accompanied with regions that have a deviating period: the spacing between dark lines in Figure 9 is sometimes as large as 6Λ . The appearance of shifted domains destroys the strict periodicity and leads to the redistribution of light over more diffraction orders (compared to the idealized simulation with 4Λ period). These domains can change in size after a switch in voltage and play a role in the device dynamics, but this is not further studied here.

At lower voltages (including 0V) for the $\Lambda = 2.9 \mu\text{m}$ region, the period observed by POM between crossed polarizers is 2Λ and diffraction appears only in half-integer and integer diffraction orders. This seems to correspond to the simulation in Figure 7 for $\Lambda = 2 \mu\text{m}$ at an intermediate voltage (5V), where strongly tilted and close to planar director regions are alternating, forming a spatial period of 2Λ and a diffraction pattern with half-integer orders (Figure 8(a)). The formation of these tilted regions depends on a delicate interplay between elastic, dielectric and surface anchoring contributions, making it difficult to accurately predict. Moreover, flexoelectric effects might play a role as well and are not taken into account in the simulations. It is however intuitively clear that regions with a strong out-of-plane director tilt will become less favorable at high voltages in the negative dielectric anisotropy range. By increasing the voltage (4 kHz) for $\Lambda = 2.9 \mu\text{m}$, the number of regions with high tilt decreases from two to one, and finally to zero per 4Λ period. For the smallest period $\Lambda = 2.1 \mu\text{m}$, the same conclusions as for $\Lambda = 2.9 \mu\text{m}$ hold at low voltages, with a 2Λ spatial period appearing in POM together with half-integer diffraction orders. This corresponds with the situation simulated for $\Lambda = 2 \mu\text{m}$ (Figure 7 and Figure 8) at intermediate voltages (5V).

5.4. Grating configuration without applied voltage

After discussing the effect of a voltage application in the negative dielectric anisotropy range, we come back to the field-free director configuration. As already mentioned in section 3, the POM image between crossed polarizers for the ideal director configuration consists of different bright (or dark) lines that are shifted over a distance $\Lambda/2$. The experimental results (Figure 3) however demonstrate that this condition is not satisfied at 0V and that deviations from the ideal configuration appear. As previously predicted by Komanduri et al.^[12a] and confirmed by our numerical simulations (Figure 5-7(a)), deviations from the ideal director configuration in gratings with small Λ/d ratio can be linked to an out-of-plane tilt of the bulk LC director. This gives rise to a 2Λ spatial period of the bulk director configuration, but when

the polarizers are oriented along the x- and y-axis respectively, the dark lines still appear with $\Lambda/2$ period in POM images. For the area with $\Lambda = 3.9 \mu\text{m}$ the dark lines are separated by a distance $\Lambda/2$ but some color difference appears between subsequent bright lines (Figure S1). The POM image observed between crossed or parallel (**Figure S4**) polarizers for $\Lambda = 3.9 \mu\text{m}$ corresponds well with the simulation (Figure 5(a)) and also the measured diffraction pattern (Figures S2), only containing 0th and -1st order, corresponds with the simulations (Figure 8).

However, the experimental observations in the gratings with smaller alignment periods $\Lambda = 2.1 \mu\text{m}$ and $\Lambda = 2.9 \mu\text{m}$ indicate that another phenomenon is occurring, because the spatial period in the POM images is 2Λ (Figure 3, Figure S1) and the diffraction pattern shows a relatively strong -0.5th order at 0V for (Figure 4 and Figure S2). This deviates from the expected diffraction pattern, only containing the 0th and -1st order, both for the ideal configuration and for the simulated 0V director configuration (Figure 8). In POM, at 0V a relatively wide ($\sim\Lambda$ width) darker area is observed between crossed polarizers in every period 2Λ (for $\Lambda = 2.1 \mu\text{m}$ and $\Lambda = 2.9 \mu\text{m}$). The POM images between parallel polarizers (Figure S4) also show a 2Λ optical period, confirming a deviation from the simulated director configuration at 0 V (Figure 6(a)). Apart from the out-of-plane tilt an additional deviation from the idealized configuration appears. As already explained in section 5.3, the 0V configuration for $\Lambda = 2.1 \mu\text{m}$ and $\Lambda = 2.9 \mu\text{m}$ can likely be explained by the appearance of local regions with a strong out-of-plane director tilt alternating with regions with a more limited director tilt. This effect is not reproduced by the simulations at 0V (Figure 6, 7), but this discrepancy might be linked to the assumption of infinite anchoring strength, the used elastic constants for the LC material (not experimentally measured), the absence of flexoelectric effects in the simulations and potential deviations between the ideal anchoring pattern and the experimentally imposed photoalignment pattern. Further research is required to accurately explain this effect and determine the dominant factors.

6. Conclusion

LC-based DOEs with enhanced optical functionality and increased efficiency are highly valuable for different kinds of photonic applications. In this article, we demonstrate very efficient (90% for circularly polarized red light) 1D diffraction over an angle of 12.6° by using a dual frequency nematic LC material in combination with a simple device design. The periodically rotating photo-alignment pattern with period $\Lambda = 2.9 \mu\text{m}$, which is slightly smaller than the layer thickness $d = 3.2 \mu\text{m}$, gives rise to a substantial out-of-plane tilt of the

LC director in the absence of an electric field. The application of a limited voltage ($4 V_{\text{rms}}$) in the frequency range with negative dielectric anisotropy allows to substantially enhance the first order diffraction efficiency (from 60% to 90%). By applying a voltage, the balance between the elastic and dielectric contribution in the free energy is shifted and the ideal director configuration can be restored by decreasing the out-of-plane tilt of the bulk director. A high diffraction efficiency over large angles has been difficult to achieve in transmissive LC gratings, and our approach provides an elegant solution that allows not only a simple device design but also electrical tunability. Apart from switching between efficient zero order transmission and first order diffraction, additional (including non-integer) diffraction orders appear at intermediate electric fields (in the frequency range with negative dielectric anisotropy). The subtle balance between the elastic and dielectric energy leads to a remarkable switching behavior that depends on the grating parameters Λ , d , the anchoring properties and the material parameters. The full potential of this mode still remains to be uncovered, but it is clear that switching of regions into a strongly tilted or a close-to-planar oriented LC configuration is the driving mechanism. The LC reorientation processes have been demonstrated with the help of finite element Q-tensor simulations for the director configuration and could be confirmed by experimental observations. All in all, the proposed grating design and described switching mechanism provide a valuable contribution to the field of LC-based DOEs. Extensions of this concept towards other optical functionalities (lenses, etc.) can be foreseen and in general this research might find widespread application in photonic devices that are using low cost, lightweight and compact optical components.

7. Experimental section/Methods

Cell fabrication and photoalignment setup: To produce the 1D LC diffraction gratings, two ITO-coated glass substrates (Delta Technologies) are glued together with a UV curable glue (Norland Optical Adhesive 68) containing spherical spacer balls with a diameter of $3 \mu\text{m}$. By recording the interference spectrum for transmitted light, the cell thickness was experimentally measured to be around $3.2 \mu\text{m}$. A photosensitive alignment layer (0.5 wt% Brilliant Yellow dissolved in DMF) was spincoated on the glass substrates (3000 rpm, 30s) and baked at 90°C for 5 min to evaporate the solvent. The glass substrates are glued together before the cell is exposed to photo-alignment illumination to define the planar anchoring pattern at the substrates. Interference illumination with the help of a left- and right- handed circularly polarized blue laser (Cobolt Twist 200, $\lambda_{\text{illum}} = 457 \text{ nm}$) beam is used to impose a periodically rotating azimuthal anchoring pattern at the substrates, defined by $\varphi(x) = \frac{\pi}{2} - \frac{\pi x}{\Lambda}$

(Figure 1), with φ the azimuthal anchoring angle with respect to the x-axis. The alignment period Λ is defined by θ_{blue} , the half-angle between the interfering beams, as $\Lambda = \frac{\lambda_{blue}}{2 \sin(\theta_{blue})}$, with $\lambda_{blue} = 457 \text{ nm}$ the wavelength of the laser that is used for illumination. The anchoring patterns (at both substrates) are inscribed by using a 120 mW illumination power during 30 s and the diameter of the illuminated spots is approximately 5 mm. Anchoring patterns with different alignment periods ($\Lambda = 2.1 \mu\text{m}$, $2.9 \mu\text{m}$ and $3.9 \mu\text{m}$) are written at different areas in the same cell.

Diffraction measurements: To analyze the behavior of the constructed LC gratings, the diffraction efficiency is measured for a helium-neon laser ($\lambda = 633 \text{ nm}$, JDS Uniphase). The linearly polarized beam ($\sim 1 \text{ mm}$ diameter) laser beam is transferred into right-handed circular polarization with a quarter wave plate. The light is incident perpendicularly to the sample and the diffracted power in transmission is measured with a photodetector. The diffraction efficiency is determined as the power in the diffraction spot divided by the power of the incident laser beam. Diffraction orders are labeled according to the diffraction equation $n_{out} \sin\theta_{out} = m \frac{\lambda}{\Lambda} + n_{in} \sin\theta_{in}$, with m the diffraction order. For perpendicular incidence, the diffraction angle in air associated with the m^{th} order is $\theta_{out} = \arcsin(m \frac{\lambda}{\Lambda})$. According to this definition, non-integer diffraction orders originate when the spatial period of the LC configuration is a multiple of the alignment period Λ that is defined at the surface of the substrates. Apart from diffraction efficiency measurements, images of the diffraction pattern on a black screen behind the sample are also taken.

Finite element Q-tensor simulations: To find the director configuration in the bulk of the device for different applied voltages, finite element Q-tensor simulations are performed.^[19] The LC is represented with the help of a second order tensor Q and the equilibrium director distribution is found by minimizing the Landau-de Gennes free energy functional. The free energy contains contributions from the elastic energy, dielectric energy and thermotropic bulk energy. The electrostatic field is determined from a variational form of Laplace's equation. Since the elastic properties of the LC material mixture 1952H are not known, we use the elastic constants for E7 ($K_{11} = 11.1 \text{ pN}$, $K_{22} = 6.5 \text{ pN}$, $K_{33} = 17.1 \text{ pN}$), and the bulk thermotropic coefficients are based on the ones measured for 5CB at a reduced temperature of -2°C , giving rise to an equilibrium order parameter of 0.54.^[10a] For the dielectric properties, a dielectric anisotropy $\Delta\epsilon = -1$ ($\epsilon_{\perp} = 5.1$, $\epsilon_{\parallel} = 4.1$) and respectively $\Delta\epsilon = 1.37$ ($\epsilon_{\perp} = 5.1$, $\epsilon_{\parallel} =$

6.47) is used in order to approximate the behavior at a frequency of 4 kHz and 1 kHz respectively at room temperature (Figure 2, Table 1). The periodically rotating surface anchoring pattern at the top and bottom substrate is taken into account using strong anchoring conditions with $\varphi(x) = \frac{\pi}{2} - \frac{\pi x}{\Lambda}$ and zero pretilt (director parallel to the xy-plane).

Simulations have been performed for the alignment periods $\Lambda = 2 \mu\text{m}$, $3 \mu\text{m}$ and $4 \mu\text{m}$. Periodic boundary conditions are used along the x-axis and a 4Λ unit cell size is simulated in order to allow pattern formation with spatial period up to 4Λ . A cell thickness $d = 3 \mu\text{m}$, similar to the experiments, is used and voltages are applied between uniform electrodes at the top and bottom substrates. To elucidate topological differences in the simulated director configurations, a representation of the LC directors on the unit sphere S^2 is provided. The director in each point in the simulation box is mapped onto the S^2 sphere and points in the mid-plane ($z = d/2$) are represented with a red color while other points are represented in blue.

Supporting Information

Supporting Information is available from the Wiley Online Library or from the author.

Acknowledgements

IN, SL and KN acknowledge funding from the Research Foundation - Flanders (FWO), grant number G0C2121N. IN also acknowledges her FWO Postdoc Fellowship, project number 1257423N. PK and OS acknowledge the financial support from Military University of Technology under research project UGB 22-801.

Received: ((will be filled in by the editorial staff))

Revised: ((will be filled in by the editorial staff))

Published online: ((will be filled in by the editorial staff))

References

- [1] a) P. Chen, Y. Q. Lu, W. Hu, *Liq. Cryst.* **2016**, *43*, 2051-2061; b) K. Kawai, M. Sakamoto, K. Noda, T. Sasaki, N. Kawatsuki, H. Ono, *J. Appl. Phys.* **2016**, *119*, 123102; c) C. Provenzano, P. Pagliusi, G. Cipparrone, *Opt. Express* **2007**, *15*, 5872-5878; d) I. Nys, V. Nersesyan, J. Beeckman, K. Neyts, *Soft Matter* **2018**, *14*, 6892-6902; e) H. Chen, Y. Weng, K. Xu, N. V. Tabiryan, S. T. Wu, *Opt. Express*. **2016**, *24*, 7287; f) Y. Weng, Y. Zhang, J. Cui, A. Liu, Z. Shen, X. Li, B. Wang, *Opt. Lett.* **2018**, *43*, 5773-5776; g) I. Nys, B. Berteloot, J.

- Beeckman, K. Neyts, *Adv. Opt. Mater.* **2022**, *10*, 202101626; h) X. Feng, L. Lu, O. Yaroshchuk, P. Bos, *Appl. Optics* **2021**, *60*, 580; i) T. Zhan, Y. Lee, G. Tan, J. Xiong, K. Yin, F. Gou, J. Zou, N. Zhang, D. Zhao, J. Yang, S. Liu, S.-T. Wu, *J. Opt. Soc. of America B* **2019**, *36*, D52-D65; j) R. Chen, Y.-H. Lee, T. Zhan, Z. An, S.-T. Wu, *Adv. Opt. Mat.* **2019**, 1900101.
- [2] a) S. Pancharatnam, *Proc.-Indian Acad. Sci. Sect. A* **1956**, *44*, 247-262; b) M. V. Berry, *Proc. R. Soc. London Ser. A* **1984**, *392*, 15-43.
- [3] a) P. Chen, B. Y. Wei, W. Hu, Y. Q. Lu, *Adv. Mater.* **2019**, *32*, 1903665; b) K. Kawai, M. Sakamoto, K. Noda, T. Sasaki, N. Kawatsuki, H. Ono, *J. Appl. Phys.* **2017**, *121*, 013102; c) I. Nys, J. Beeckman, K. Neyts, *Soft Matter* **2015**, *11*, 7802-7808; d) M. Stebryte, I. Nys, J. Beeckman, K. Neyts, *Opt. Express* **2022**, *30*, 42829.
- [4] a) O. Yaroshchuk, Y. Reznikov, *J. Mater. Chem.* **2012**, *22*, 286; b) V. Chigrinov, *Crystals* **2013**, *3*, 149–162.
- [5] a) E. A. Shteyner, A. K. Srivastava, V. G. Chigrinov, H.-S. Kwok, A. D. Afanasyev, *Soft Matter* **2013**, *9*, 5160; b) S. Liu, I. Nys, K. Neyts, *Adv. Opt. Mater.* **2022**, *10*, 2200711; b) 1, C. D. Author 2, *Adv. Mater.* **2020**, *18*, 2001086; c) S. Cho, H. Yoshida, M. Ozaki, *Opt. Express* **2022**, *30*, 1607; d) X. Xiang, J. Kim, R. Komanduri, M. J. Escuti, *Opt. Express* **2017**, *25*, 19298-19308.
- [6] a) G. P. Crawford, J. N. Eakin, M. D. Radcliffe, A. Callan-jones, R. A. Pelcovits, *J. Appl. Phys.* **2005**, *98*, 123102; b) T. Zhan, J. Xiong, Y.-H. Lee, R. Chen, S.-T. Wu, *Opt. Express* **2019**, *27*, 2632-2642.
- [7] a) M. N. Miskiewicz, M. J. Escuti, *Opt. Express* **2014**, *22*, 12691; b) M. N. Miskiewicz, M. J. Escuti, *Opt. Eng.* **2015**, *54*, 025101.
- [8] C. Culbreath, N. Glazar, H. Yokoyama, *Rev. Sci. Instrum.* **2011**, *82*, 126107.
- [9] Y. Guo, M. Jiang, C. Peng, K. Sun, O. Yaroshchuk, O. Lavrentovich, Q.-H. Wei, *Adv. Mater.* **2016**, *28*, 2353.
- [10] a) B. Berteloot, I. Nys, G. Poy, J. Beeckman, K. Neyts, *Soft Matter* **2020**, *16*, 4999-5008; b) Y. Li, Y. Liu, S. Li, P. Zhou, T. Zhan, Q. Chen, Y. Su, and S.-T. Wu, *Opt. Express* **2019**, *27*, 9054; c) L. De Sio, D. E. Roberts, Z. Liao, S. Nersisyan, O. Uskova, L. Wickboldt, N. Tabiryan, D. M. Steeves, *Opt. Express* **2016**, *24*, 18297-18306.
- [11] a) J. Kobashi, H. Yoshida, M. Ozaki, *Nat. Photon.* **2016**, *10*, 389-392; b) I. Nys, M. Stebryte, Y. Ye Ussembayev, J. Beeckman, K. Neyts, *Adv. Opt. Mater.* **2019**, *7*, 1901364; c) M. Stebryte, I. Nys, Y. Ye Ussembayev, J. Beeckman, K. Neyts, *Crystals* **2020**, *10*, 807; d) Y. H. Lee, K. Yin, S. T. Wu, *Opt. Express* **2017**, *25*, 27008-27014.

- [12] a) R. K. Komanduri, M. J. Escuti, *Soft Matter Phys.* **2007**, 76, 021701; b) I. Nys, *Liq. Cryst. Today* **2021**, 29, 65-83.
- [13] a) K. Gao, C. McGinty, H. Payson, S. Berry, J. Vornehm, V. Finnemeyer, B. Roberts, P. Bos, *Opt. Express* **2016**, 25, 6283-6293; b) H. Cheng, A. K. Bhowmik, P. J. Bos, *Appl. Opt.* **2015**, 54, 10035; c) C. Oh, M. J. Escuti, *Opt. Lett.* 2008, 33, 2287-2289; X. Xiang, J. Kim, M. J. Escuti, *Scientific Rep.* 2018, 8, 10-15.
- [14] a) W. Duan, P. Chen, B.-Y. Wei, S.-J. Ge, X. Liang, W. Hu, Y.-Q. Lu, *Opt. Mat. Exp.* **2016**, 6, 597.
- [15] R. Dąbrowski, M. Celiński, O. Chojnowska, P. Kula, J. Dziaduszek, S. Urban, *Liquid Crystals* **2013**, 40, 1339-1353.
- [16] G. Poy, S. Zumer, *Opt. Express* **2020**, 28, 24327-24341.
- [17] M. J. Escuti, W. M. Jones, *SID Symp. Digest* **2006**, 37, 1443-1446.
- [18] S. Liu, H. Yu, M. Jiang, J. Feng, Q.-H. Wei, *J. Opt. Soc. Am. B* **2023**, 40, 431-435.
- [19] a) R. James, E. Willman, F.A. Fernández, S. E. Day, *IEEE Trans. Electron Devices* **2006**, 53, 1575-1582; b) R. James, E. Willman, R. Ghannam, J. Beeckman, F.A. Fernández, *J. Appl. Phys.* **2021**, 130, 134701.

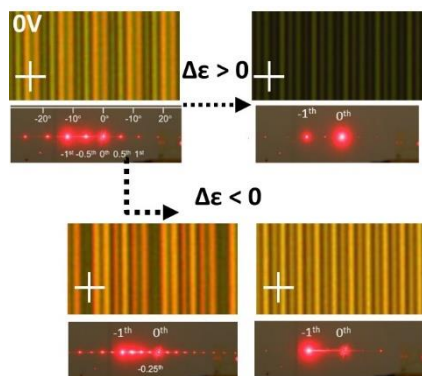
The table of contents entry should be 50–60 words long and should be written in the present tense. The text should be different from the abstract text.

Photo-patterned surface anchoring is successfully used to generate liquid crystal flat optical components that work based on the geometric phase principle. Dual frequency liquid crystal allows to substantially enhance the optical performance of the generated gratings. The diffraction efficiency over large angles is strongly enhanced and additional tunability is achieved by adjusting the frequency and amplitude of the applied electric field.

I. Nys*, S. Liu, Y.-N. Huang, O. Strzeczysz, P. Kula and K. Neyts

Geometric phase flat optical gratings with high diffraction angle based on dual frequency nematic liquid crystal

ToC figure ((Please choose one size: 55 mm broad \times 50 mm high **or** 110 mm broad \times 20 mm high. Please do not use any other dimensions))



Supporting Information

Geometric phase flat optical gratings with high diffraction angle based on dual frequency nematic liquid crystal

*Inge Nys**, *Sunqian Liu*, *Yu-Nung Huang*, *Olga Strzeżysz*, *Przemysław Kula* and *Kristiaan Neyts*

Anchoring patterns with different alignment periods ($\Lambda = 2.1 \mu\text{m}$, $2.9 \mu\text{m}$ and $3.9 \mu\text{m}$) are written at different areas in the same cell. The analysis in the manuscript is mainly focused on the alignment period $\Lambda = 2.9 \mu\text{m}$, while additional results for $\Lambda = 2.1 \mu\text{m}$ and $3.9 \mu\text{m}$ are reported in the supporting information to provide a broader insight in the device behavior.

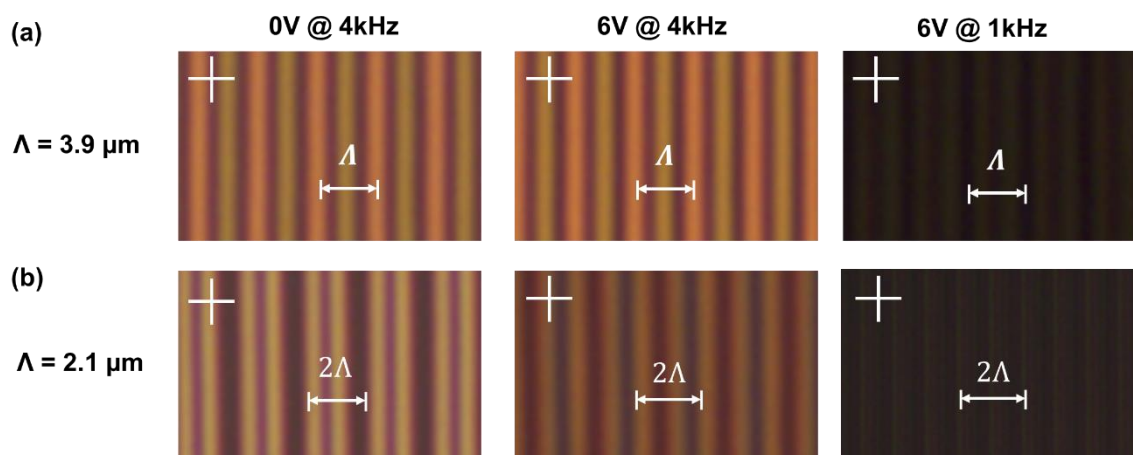


Figure S1. POM images between crossed polarizers for 0V and 6V with an ac frequency of 4 kHz and 1 kHz applied respectively. Results for the 1D gratings with alignment period $\Lambda = 3.9 \mu\text{m}$ (top) and $\Lambda = 2.1 \mu\text{m}$ (bottom) are shown. POM images for alignment period $\Lambda = 2.9 \mu\text{m}$ are given in Figure 3 of the manuscript.

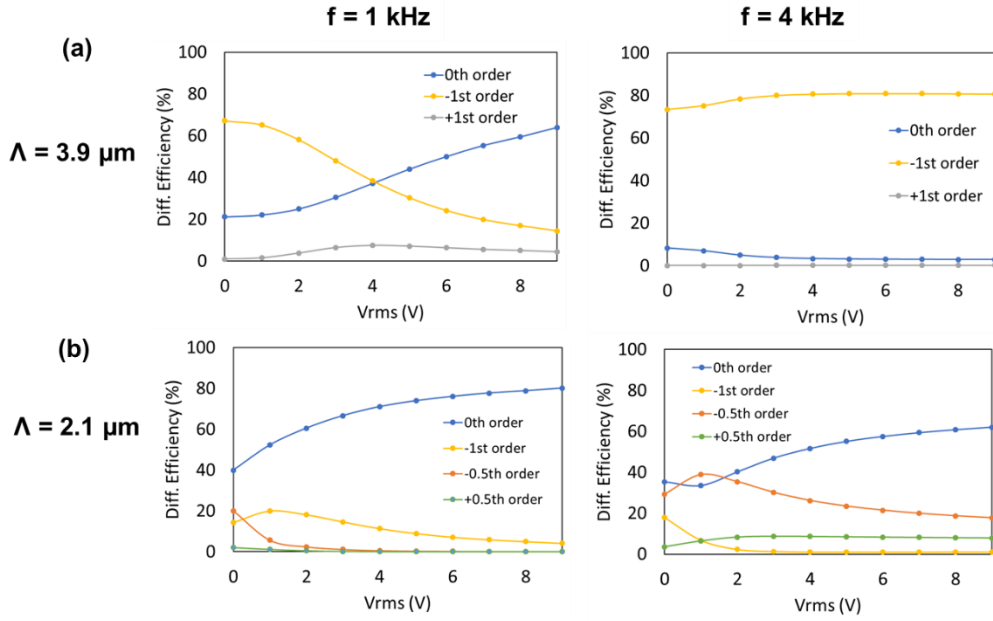


Figure S2. (a) Experimentally measured diffraction efficiencies as a function of the voltage in different diffraction orders, for frequencies 1 kHz ($\Delta\epsilon > 0$) and 4 kHz ($\Delta\epsilon < 0$) of the applied electric field. Measurements for alignment period $\Lambda = 3.9 \mu\text{m}$ (a) and $\Lambda = 2.1 \mu\text{m}$ (b) are shown. Measurements for alignment period $\Lambda = 2.9 \mu\text{m}$ are given in Figure 4 of the manuscript.

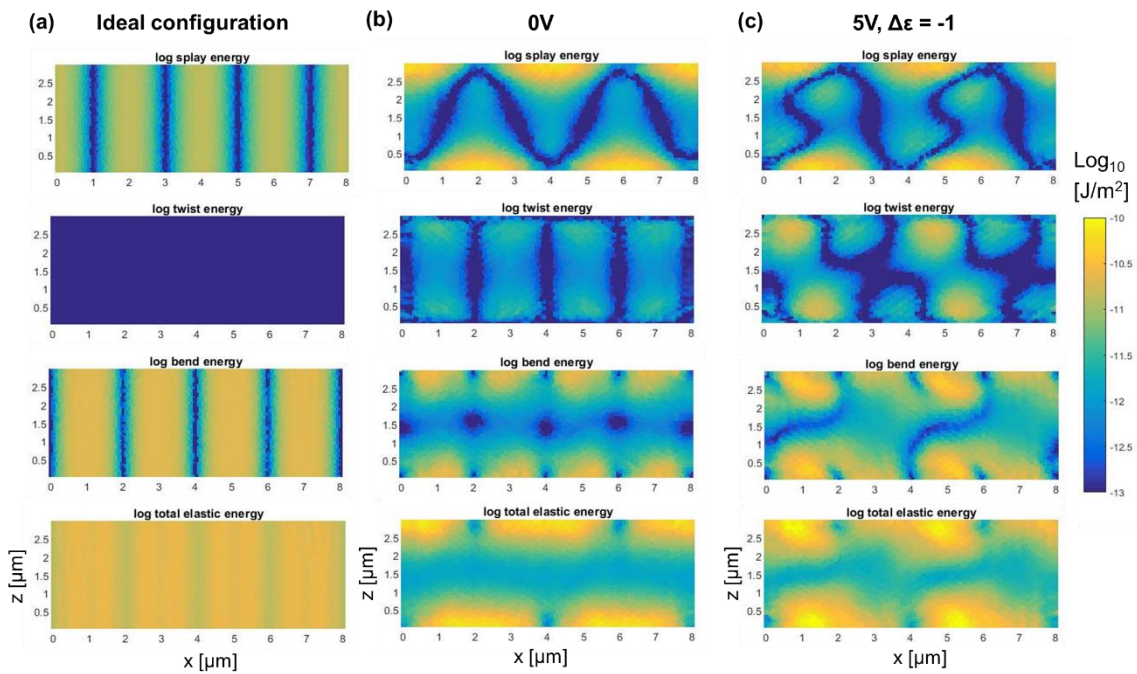


Figure S3. (a) Splay, twist, bend and total elastic energy (from top to bottom) for the ideal director configuration (Figure 1(a)). (b,c) Simulated splay, twist, bend and total elastic energy (from top to bottom) for the simulated director configurations shown in Figure 7(a) at 0V and

Figure (c) at 5V with $\Delta\epsilon = -1$. The grating period is $\Lambda = 2 \mu\text{m}$ and cell thickness is $d = 3 \mu\text{m}$.

A logarithmic scale is used in the color bar. The elastic constants of E7 are used.

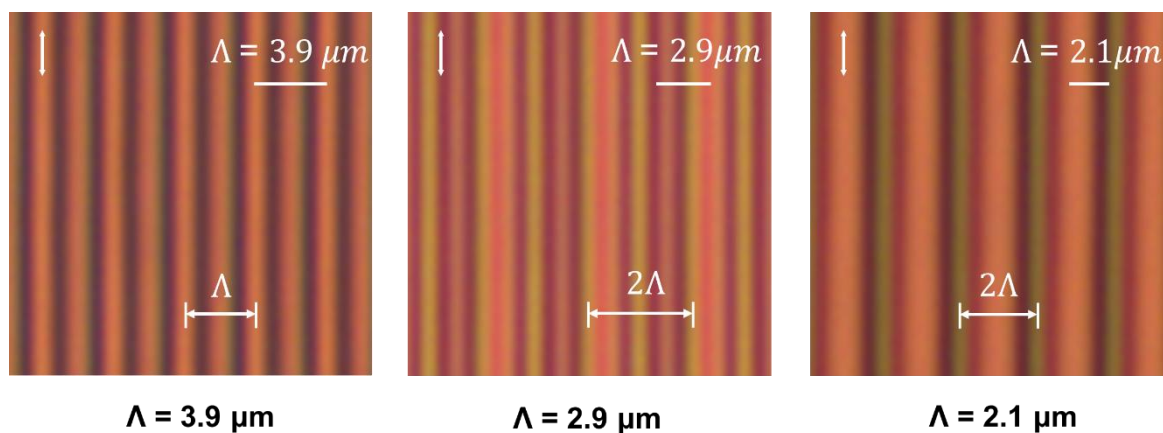


Figure S4. POM images between parallel polarizers, oriented along the y-axis, for the three different alignment periods $\Lambda = 3.9 \mu\text{m}$, $\Lambda = 2.9 \mu\text{m}$ and $\Lambda = 2.1 \mu\text{m}$. No voltage was applied to the cell.